Quality of Fingerprint Scans captured using Optical Coherence Tomography

Ctirad Sousedik
NISlab, Gjøvik University College
Teknologiveien 22, 2815 Gjovik, Norway
ctirad.sousedik@hig.no

Christoph Busch
NISlab, Gjøvik University College
Teknologiveien 22, 2815 Gjovik, Norway
christoph.busch@hig.no

Abstract

The performance limitations of the state-of-the-art methods for fingerprint presentation attack detection motivate the application of the Optical Coherence Tomography as the scanning technology capable of capturing all the information necessary for both the fingerprint identification and the presentation attack detection. The previous research has evidenced the need for a reliable technique for assessing quality of the captured scans so that the compliance of the capture subject behavior with acquisition rules could be verified. Good quality of these scans is not only a precondition of good system performance but it also enables reliable processing of the scanned data in the first place. This paper's contribution consists of a novel approach for estimation of the layered structure of an OCT fingerprint scan as a set of analytical surfaces and a subsequent analysis of the quality property of the obtained scan that is related to non-compliant behavior of the capture subjects. The method was able to detect 98% *of low-quality scans at a false detection rate of* 3%.

1. Introduction

Fingerprint biometrics are being increasingly applied as a means of access control to sensitive facilities or data sources, which motivates the development of a highly secure fingerprint identification technology capable of unsupervised operation that is resistant to moderate or high attack potential [12].

Due to wide application of fingerprint biometrics, a large number of techniques and approaches have been developed in order to produce artificial fingerprints capable of deceiving the state-of-the-art fingerprint identification systems. In parallel, significant research effort has been invested into the development of Presentation Attack Detection (PAD) methods that would allow for a reliable application of fingerprint biometrics in terms of security [4][8][5].

Despite of the significant research efforts so far, the PAD methods have not provided for convincing results, if a targeted attack by using a fingerprint artefact designed specifically to deceive a particular sensor technology is considered [15][5].

Based on whether or not a specific PAD method requires extra sensors in addition to the original 2D fingerprint data, the PAD approaches can be divided into two groups [2]. The authors of [15] argue that the 2D scans yielded by the state-of-the art sensors might not be sufficient to develop a reliable PAD approach, if high-quality artefacts, produced by means of novel methods and materials, are considered. The hardware-based PAD approaches can be vulnerable, if only a limited number of properties of the genuine fingers are being verified, as the attacker can design the artefact fingerprint such that it possesses the specific small set of critical properties. Analysis of a larger number of properties is possible, but the resulting complexity requires application of machine learning techniques in order to deal with the widely varying properties of human fingers. As the outcomes of the machine learning techniques are strongly dependent on the training data available during the design phase, the resulting PAD methods can still be vulnerable if a very novel artefact fingerprint is used [15].

The above mentioned challenges have motivated a search for a fingerprint sensing technology that could provide for all the information needed for both the fingerprint identification and the PAD functionality in a single scan. In addition, the PAD related information should be ideally present in a graspable manner such that the PAD method could be developed without machine learning using a known set of artefact samples.

A promising technology in terms of the above mentioned properties is the Optical Coherence Tomography (OCT) [10]. The OCT allows for acquisition of high-resolution 3D volumetric scans of the fingerprint tissue, up to depth of 2-3 mm. In addition to capturing the outer fingerprint pattern, the OCT scan contains representation of the inner fingerprint pattern responsible for the stability and regeneration of the outer fingerprint pattern, as well as tiny structures such as sweat glands.

The recent efforts into the development of a secure OCT-

based fingerprint recognition technology have revealed a benefit of a reliable quality control method that would validate certain properties of the OCT scans [10]. In order to ensure the reliable functionality of the fingerprint recognition and PAD pipelines, only the OCT scans with acceptable quality-related properties could be further analyzed. In case of a non-compliant user behavior, the OCT scans contain specific patterns in the 3D volumetric scans that would be difficult or sub-optimal to analyze using the fingerprint quality methods designed for 2D fingerprint scans.

This paper's contribution consists in suggesting a fast and reliable approach to detection of the layers in the OCT scan that contain the outer and inner fingerprint patterns, their extraction, and a subsequent assessment of the quality of the extracted fingerprints in terms of OCT-specific quality degradations.

The paper is organized as follows: The section 2 discusses the application of the OCT for the fingerprint sensing scenario. The section 3 describes the database used in this work and proposes a novel method for estimating the layered structure of the OCT fingerprint scan along with an approach for assessing the quality of the scans in terms of compliant capture subject behavior. The next section 4 evaluates the performance of the proposed approach and the final section 5 summarizes the results and suggests directions for future work.

2. Optical Coherence Tomography for fingerprint sensing

The OCT is a scanning technology - originally developed for medical purposes - that can acquire 3D volumetric representations of the scanned material up to 2-3 mm under the surface as a function of its local scattering properties. The OCT typically operates with infrared wavelengths of the spectrum [10].

The potential of the OCT technology for the fingerprint sensing scenario was researched by the project *OCT-Finger* [13]. The study has confirmed the ability of the technology to visualize the inner structure of the genuine human fingers, as well as the artefact representations. The OCT was capable of capturing the outer fingerprint surface along with the inner fingerprint pattern that copies its structure and allows for its regeneration and stability. In addition, the study has demonstrated the ability of the OCT technology to visualize the fine structures of the sweat glands that are responsible for generation of sweat fluids in human fingers [10]. For the artefact representations, the OCT was capable of capturing the outer and inner structure of the artefact material and could also capture the original finger structure of the attacker, who was wearing a thin-layered artefact on his finger [10]. Classification into genuine and artefact fingers, carried out by employing a test-group of individuals, provided for almost 100% classification accuracy, which demonstrates the OCT technology's potential for providing a sufficient amount of information for a reliable PAD method [10]. It can be assumed that replicating the structure of a genuine OCT fingerprint scan by means of an artefact would be extremely difficult. The above mentioned properties demonstrate the potential of the technology not only for PAD solutions, but also in terms of increasing the reliability of the OCT scanning in conditions that are difficult for the current fingerprint sensors (e.g. optical TIR sensors), such as too dry, wet or oily fingers.

Nevertheless, the initial attempts to develop a fingerprint PAD method using the OCT [11] in terms of the *OCT-Finger* [13] have revealed a number of challenges. The size of the volumetric data grows very quickly with the scanning resolution and the size of the scanning area. The size of the data would represent a full fingerprint area of 2×2 cm at the resolution necessary to observe the fine sweat gland structures, is about 1GB, given that a voxel is encoded by a single byte. This renders a great challenge both in terms of speed of the scanning procedure and the data processing pipeline, as the entire process has to be finished in terms of seconds as required by the practical fingerprint sensing scenarios. In addition, the inner structure and scattering properties of genuine human fingers are not homogeneous. The subjects have widely varying densities of sweat glands and their specific structure. The OCT technology also captures the fingerprint structure with a significant amount of speckle noise and occasional faulty measurements.

The study [10] has also revealed additional challenges as regards the quality of the acquired representations related to non-compliant behavior of the capture subjects, as more than 10% of the scans were of insufficient quality - Fig. 6,7,8. The finger needed to have been held still on the OCT sensor for a period of time ($<$ 3s), and low-quality scans were acquired when the fingers had been shaken or lifted off during the capture process. The issue can be partly mitigated by shortening the scanning period and improving the hardware design in terms of the stability of the scanned finger, however, it is difficult to completely remove the negative effects in this way. An OCT fingerprint scan quality assessment would provide for a validation of the expected scan structure, greatly supporting the reliability of the PAD method applied.

3. OCT scan quality estimation

3.1. Database

The in-house semi-public OCT scan database used in this work has been composed within the framework of the *OCT-Finger* [10]. The OCT scanning device was based on the Fourier-Domain OCT (FD-OCT) technology with an acquisition time of $2.24s$ per scan and operating on a wavelength of $1300 \pm 55nm$. A scan represents $4 \times 4 \times 2.5mm$-

large volume ($width \times height \times depth$) of the fingertip at a resolution of $200 \times 200 \times 512$ voxels.

The scans of genuine living fingers represent fingers of 226 subjects of which 96 (42%) were males and 130 (58%) females. The age structure has been as follows: 18 subjects (8%), 5-20 years; 96 subjects, 20-40 years (42%); 76 subjects (34%), 40-60 years; 36 subjects (16%), 60-80 years. For each subject, at least the right thumb, the right index finger and the right little finger was scanned. Each finger instance was scanned 11 times, which provided for the minimum total amount of 7458 samples of genuine living finger scans.

The fake fingerprint scans represent 30 different classes of artefact fingerprints. The artefacts differ in the mold material composition (gelatin, silicone, latex, window paint, wood glue etc.) and the actual artefact material composition (glycerol, graphite, window paint etc.). For each class, at least 9 artefact fingerprints were produced. Each of the artefact fingerprints was used to acquire at least 11 scans, yielding for minimum number of 2970 artefact fingerprint scans.

In addition to that, fingers of 5 male and 5 female dead bodies were scanned. For each body, 3 fingers were scanned, 11 times each, providing for 330 dead finger samples.

3.2. OCT scan structure

The OCT scanner generates a 3D volumetric representation of the scanned finger. The capture device is observing scattering properties and effectively measuring the amount of light reflected from each point in the scanned volume (see Fig. 1 for an illustration of the scanning procedure). The typical structure of an OCT scan of a genuine finger is shown by Fig. 2. The outer surface of the finger generates a thin layer of strong reflections that provide for a highly detailed representation of the 3D structure of the outer fingerprint pattern. The following layer represents reflections from beneath the outer surface and captures the fine structure of the sweat glands. The next layer of voxels of stronger reflections represents the structure of the inner fingerprint at the dermis boundary, from which the identical ridge flow pattern can be observed. Anatomically, the structure of the inner fingerprint pattern provides the mother template from which the outer fingerprint regenerates, ensuring its reproducibility after cuts and other minor injuries. The depth range of the sweat gland layer as well as the length of the sweat glands varies among different subjects. The density of the sweat glands varies strongly, having 10 times more sweat glands in some subjects compared to others. The structure of a sweat gland can be described as a helix with some degree of random biological variations.

The inner fingerprint cell structure does not provide for a thin, boundary-like layer as the outer fingerprint. It

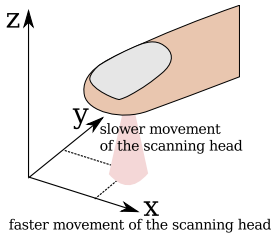

Figure 1. Schematic representation of the OCT scanning procedure

rather yields a point cloud of voxels of stronger reflections that copy the outer fingerprint pattern with some degree of spreading over a limited depth range. The strong-response voxels are concentrated over the fingerprint ridges, while the fingerprint valleys provide for significantly weaker responses, often indistinguishable from reflections generated by the surrounding tissue.

In order to analyze the OCT fingerprint scans in an automated manner, a fast and reliable approach for extracting the layered structure of the scans is needed.

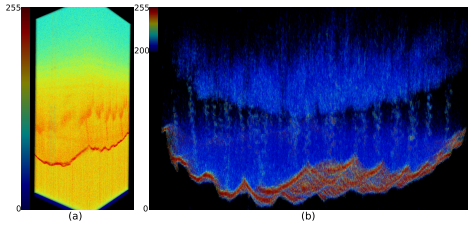

Figure 2. (a) heat-map visualization of an OCT scan of a genuine finger (b) OCT scan of a genuine finger, voxels with values below 200 rendered transparent [14]

3.3. Robust estimation of fingerprint layer positions

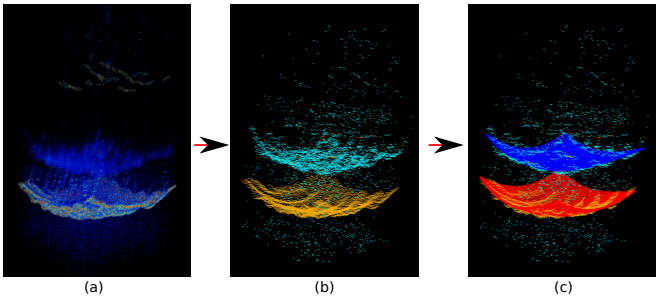

Figure 3. Pipeline of the estimation of the fingerprint layer positions (a) OCT scan of a genuine fingerprint (b) Initial candidate point sets; yellow $\rightarrow S_{outer}$, azure $\rightarrow S_{inner}$ (c) Smooth surfaces fitted to the main cluster of points in the candidate point sets; red $\rightarrow z = f^{outer}(x, y)$, blue $\rightarrow z = f^{inner}(x, y)$

Initially, two sets of candidate points, S_{inner} and S_{outer}, are extracted from the original OCT scan, representing a densely assembled cloud of points that are - in a vertical perspective - centered around outer and inner fingerprint layers.

This work was inspired by a method published by Sousedik et. al [14] that provided for an efficient approach to localize spatial positions that are members of the said cloud. The method of Sousedik et al. is a fast method for the approximation of layer positions in volumetric data performed by analysis of phases and amplitudes of overlapping sinusoidal window functions. In our work, we analyze every column of $3 \times 3 \times 512$ voxels to detect a candidate point for each of the two layers (Fig. 3a).

The resolution of $3 \times 3 \times 512$-voxel columns allows for obtaining the details of the fingerprint pattern captured by the OCT scan, both in terms of the outer and the inner fingerprint layers. However, the method by Sousedik et al. [14] generates a number of outliers. Especially for the inner fingerprint pattern, a large number of outliers is being generated, as some of the layer detection columns go through the fingerprint valleys, which, for the inner fingerprint, often do not generate significantly stronger responses as compared to the surrounding tissue (Fig. 3b). Nevertheless, a clearly sufficient number of correctly placed layer candidate points are found for both of the fingerprint layers, as long as the quality of the OCT scan is acceptable.

This fact suggests a statistical approach capable of fitting a smooth surface, $z = f^{(l)}(x, y)$, to the main cluster of the detected points, $\mathbf{x}^{(l)} = (x^{(l)}, y^{(l)}, z^{(l)}) \in S_{(l)} \wedge l \in \{inner, outer\}$. However, there are number of challenges to cope with; Even though the strong and clear reflection from the outer fingerprint surface typically provides for a clearly identifiable layer, both of the candidate point sets, S_{outer} and S_{inner}, still contain a significant number of outliers whose influence on the final smooth surface has to be eliminated (Fig. 3b). In addition, the non-outlier candidate points do not lie precisely on a smooth surface. For the outer fingerprint, the non-outlier candidate points, $\mathbf{x}_i^{outer} \in S_{outer}$, follow the 3D structure of the fingerprint, and hence these points vary around the desired smooth surface (Fig. 3c). For the inner fingerprint, the tissues are captured as a point cloud of stronger responses, providing for a somewhat randomly varying positions of the detected candidate points, $\mathbf{x}_i^{inner} \in S_{inner}$, after the initial layer estimation method has been applied at the higher resolution of 3×3 voxels wide columns (Fig. 3b). Given the strong time constraints required by practical applications, the resulting approach needs to provide for high accuracy of the fitting procedure at very limited computational costs.

The direct application of surface fitting methods, such as Levenberg-Marquardt [9], is sub-optimal, as this would yield inaccurate results due to the significant number of outliers present in the candidate points sets. The typically applied RANSAC-based approaches [1] are well-suited for dealing with outliers, however their efficiency and accuracy is sub-optimal if the non-outlier points do not lie very closely to the fitted surface. In addition, the RANSAC-based approaches require a clearly defined mathematical model of the fitted surface, with a limited number of degrees of freedom, if an efficient computation is expected. These properties do not support the application of the RANSAC-based approaches for this scenario, due to the number of degrees of freedom necessary to model the fingerprint surface, and the fact that the candidate points lie very rarely exactly on the fitted surface.

Followingly, we have developed a method for smooth surface estimation by means of an innovative procedure for neural network training. We have modeled the smooth surface, $z = f^{(l)}(x, y) \wedge l \in \{inner, outer\}$, using a back-propagation neural network [3] with a single hidden layer containing 4 neurons, as illustrated by Fig. 4. The network

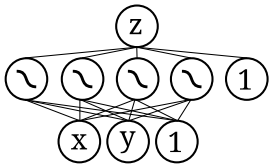

Figure 4. Structure of the fingerprint layer estimation neural network

consists of 2 input neurons, 4 hidden neurons, and one output neuron. Both the input neurons and the hidden neurons have each an associated bias neuron. This network is trained to effectively represent the smooth fingerprint surface as a function $z = f^{(l)}(x, y) \wedge l \in \{inner, outer\}$, where z represents the depth of the fitted surface at the point (x, y). All the hidden neurons consist of a Gaussian transfer function defined as $z = e^{-x^2 s^2}$, where s is the steepness value. The structure of the neural network expresses the function $z = s(w_{12}e^{-(w_0 x + w_1 y + w_2)^2 s^2} + w_{13}e^{-(w_3 x + w_4 y + w_5)^2 s^2} + w_{14}e^{-(w_6 x + w_7 y + w_8)^2 s^2} + w_{15}e^{-(w_9 x + w_{10} y + w_{11})^2 s^2} + w_{16})$, and allows to represent the variations of the shape of the human finger surface, while disregarding the influences of the fingerprint pattern present in the outer fingerprint candidate point set, S_{outer}, or influences of the somewhat random variations present in the inner fingerprint candidate point set, S_{inner}. The limited number of neurons allow for a computationally inexpensive training procedure.

In order to successfully deal with the negative influences of the outlier candidate points, the neural network would have to converge to the main cluster of the candidate points, fitting an approximation surface to these points, while disregarding the influences of the outliers. This cannot be achieved by standard procedures for neural network training, as these standard procedures consider influences of all of the data points on the resulting surface.

We addressed the problem by developing the following training procedure:

1. Initialize the weights of the neural network such that

it represents an average expected surface of the fingerprint

2. Perform k steps of the backpropagation training procedure in order to converge to a surface that represents all the candidate points, $\mathbf{x}_i^{(l)} \in S_{(l)}$, in a particular set, $l \in \{inner, outer\}$, including the outlier points ($k = 50$)

3. Perform one step of the backpropagation training procedure using the candidate point set $S_{(l)}$, with x and y normalized to $(0, 1)$

4. Evaluate the z-distance of the candidate points from the currently estimated surface, $d_i^{(l)} = |z_i^{(l)} - f^{(l)}(x_i^{(l)}, y_i^{(l)})|$, and remove the points whose distance is larger than d_{max} from the set $S_{(l)}$

5. Decrease the d_{max} by an amount Δd ($\Delta d = 0.075/n$)

6. Repeat the steps 3, 4 and 5, n times ($n = 50$)

The resulting functions denormalized into $[0, depth - 1]$, $z = f^{(l)}(x, y) \wedge l \in \{inner, outer\}$, represent the smooth surfaces fitted to the inner and outer fingerprint candidate points.

The above formulated algorithm represents a training procedure that causes the neural network gradually to disregard the influence of certain training data points as the training progresses. Thus the algorithm ensures that the surface, represented by the network, is converging to an approximation of the most significant cluster of the training data points. For the scenario analyzed in this paper, the network's surface converges to the main cluster of correctly identified candidate points, gradually disregarding the influence of the outliers in the course of the training (Fig. 3c). The detected outer and inner fingerprint of a good quality scan is shown in Fig. 5.

The above proposed approach for extraction of the layered structure of an OCT fingerprint scan provides a basis for automated assessment of its quality.

3.4. OCT scan quality estimation method

The agency that has kindly provided the *BSI-OCT-1-FINGER* database has indicated that OCT fingerprint scan quality problems were noted during the data collection [10]. Although high quality scans had typically been captured, a number of effects that are specific to the OCT fingerprint scanning procedure degraded the quality severely. A considerable subset of the capture subjects showed a tendency to lift their fingers too early from the sensor, or change their finger positions during the capture process. Especially, a pattern caused by irregular shaking of the fingers is commonly found in low-quality scans. For the current capture devices and their scanning durations, it is a challenge for the capture subject to hold the finger still during the scanning period, which can result in incomplete scans or strong distortions of the detected surfaces (see Fig. 6, 7). In addition, pressing the finger too hard against the scanner surface resulted in incomplete capturing of the layer surfaces in the acquired OCT fingerprint scans. We

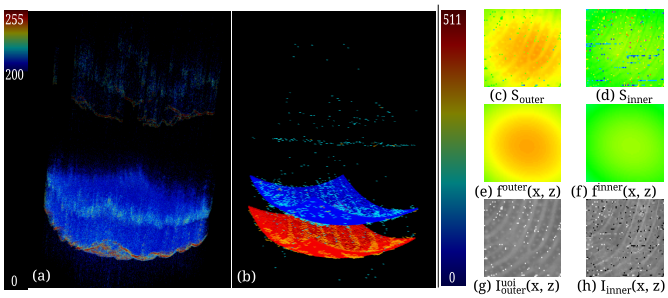

Figure 5. Visualization of the OCT quality estimation method for a a scan of excellent quality - outliers are caused almost solely by the OCT scan noise and the inherent unclarity of the inner fingerprint

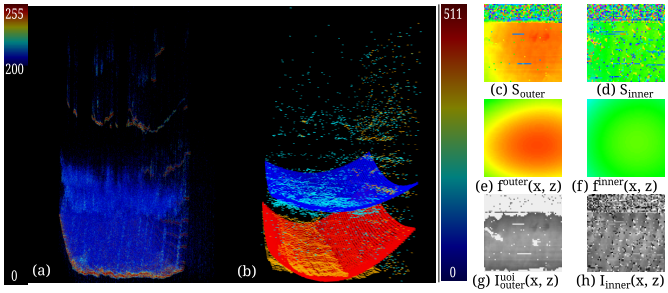

Figure 6. Visualization of the OCT quality estimation method for a scan, for which the scanned finger was lifted off too early from the sensor

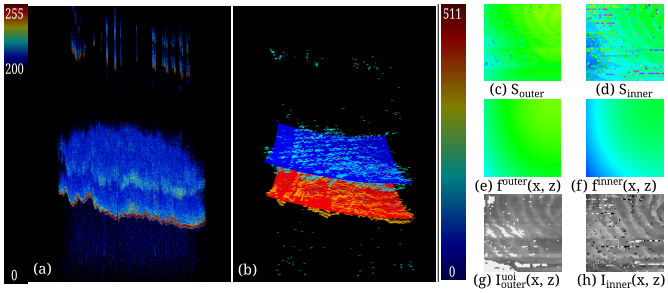

Figure 7. Visualization of the OCT quality estimation method for a scan that resulted from strong shaking the scanned finger

have assigned the OCT-specific scan quality issues into two classes, namely $C_{strong-defect}$ and $C_{medium-defect}$. The first class takes into account large distortions, caused by lifting the fingers too early, strongly shaking the fingers and pressing them too hard against the surface of the OCT sensor. In such instances of non-compliant capture subject behavior, the OCT scans provide for sets of candidate points,

S_{inner} and S_{outer}, where the distances, $d^{(l)}_{outlier}$, of the outlier points from the approximation surfaces, $f^{(l)}(x,y) \wedge l \in \{inner, outer\}$, will be much larger than the distances, $d^{(l)}_{inlier}$, caused by the presence of the fingerprint pattern in the outer fingerprint layer, or much larger than the random variations present due to the point-cloud nature of the inner fingerprint layer:

$$d^{(l)} = |z - f^{(l)}(x,y)| \wedge d^{(l)}_{outlier} > d^{(l)}_{inlier} \quad (1)$$

The second class of the scan quality problems, $C_{medium-defect}$, is related to slight shaking of the finger during the acquisition process (see an example in Fig. 8). In this case, the distances of candidate points, $d^{(l)}$, are within the expected distance range:

$$d^{(l)} = |z - f^{(l)}(x,y)| \wedge d^{(l)} \leq d^{(l)}_{inlier} \quad (2)$$

Nevertheless, the variations can still be spotted due to the

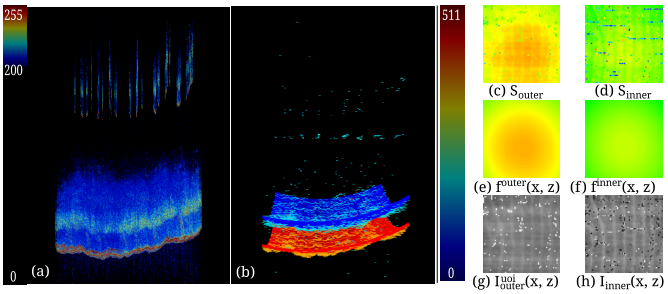

Figure 8. Visualization of the OCT quality estimation method for a scan that resulted from slight shaking the scanned finger

nature of the movement of the OCT scanning head. The scanning head moves very fast along one axis, but much slower along the opposite axis, as the latter's coordinate is adjusted upon completion of every single line scan (see Fig. 1). These variations can be approximated by the following equation that describes the z coordinate of the layer candidate points, $(x,y,z) \in S_{(l)}$:

$$z_{LowQuality} = z_{real} + g(y) \quad (3)$$

where y is the coordinate that represents movement along the axis in which the scanning head moves slower, always upon completion of the scanning along the x axis. Due to the high speed of the head along the x axis, the resulting changes in positions of the layer candidate points can be approximated as being constant for every x coordinate. This provides for a shaking approximation function, $g(y)$, that describes the shaking pattern along the changes of the y coordinate.

For further analysis, we extract a 2D fingerprint estimation image for both the outer and the inner fingerprint, $I_{(l)}(x,y)$, as follows (Fig. 5(g) and (h)):

$$I_{(l)}(x,y) = z^{(l)} - f^{(l)}(x^{(l)}, y^{(l)}) \quad (4)$$

where $(x^{(l)}, y^{(l)}, z^{(l)}) \in S_{(l)} \wedge l \in \{inner, outer\}$.

Because the Fourier-Domain OCT (FD-OCT) scanning head captures the entire line-scan along the z axis at one point in time, the inner fingerprint estimation image, $I_{inner}(x,y)$, is subject to the same OCT-specific effects, caused by the non-compliant capture subject behavior, as the outer fingerprint estimation image, $I_{outer}(x,y)$. Due to the point-cloud nature of the inner fingerprint layer, the clearer, boundary-like outer fingerprint layer provides for a more reliable basis for the resulting OCT-specific quality estimation, while the inner fingerprint estimation image, $I_{inner}(x,y)$, can be used for further processing as regards fingerprint analysis and 2D-based quality detection methods.

The high-quality OCT scans can often be distinguished from the low-quality scans based on the number of outliers in $I_{outer}(x,y)$. However, these outliers typically represent various random depth values, which fact is not ideal in terms of considering the influences of the outliers equally. In order to unify the influences of the outliers, the image with uniform outlier influences, I^{uoi}_{outer}, is computed as follows:

$$I^{uoi}_{outer}(\mathbf{x}) = \begin{cases} I_{outer}(\mathbf{x}) & \text{if } |I_{outer}(\mathbf{x})| \leq \frac{1}{2} F d_{max} \\ 250 & \text{if } |I_{outer}(\mathbf{x})| > \frac{1}{2} F d_{max} \end{cases} \quad (5)$$

where $Fd_{max} = 30$ is the maximum depth of a human fingerprint, defined as slightly larger $(600\mu m)$ than the inter-ridge distance for the Caucasian population $(500\mu m)$ [7].

We define the first OCT-scan quality score, qs_1, that describes the class of more severe quality problems, related to lifting the fingers too early, pressing them too hard against the sensor surface or shaking them excessively. As our intention is to formulate a quality metric according [6], the qs_1 is defined as the amount of variations in y-axis frequencies lower than the frequency of the fingerprint, as follows:

$$qs_1 = 100 - \min(100, \frac{1}{2} \operatorname{std}(G_y(\frac{1}{w} \sum_{x=1}^{w} I^{uoi}_{outer}(x,y)))) \quad (6)$$

where G_y is a Gaussian filter, varying in y-axis only, ($\sigma = 7$) of size 1×11 pixels and std is the standard deviation.

The second quality score, qs_2, deals with the mild shaking of the fingers during the scanning period. Due to the model that has been described by the equation (3), a pattern is observable in the outer fingerprint image $I_{outer}(x,y)$ that resembles stripes of changing brightness added to the image (Fig. 8 (c) and (g)).

In order to minimize the influences of the outliers, the cleared image, $I^{cleared}_{outer}$, is defined as follows:

$$I^{clared}_{outer}(\mathbf{x}) = \begin{cases} I_{outer}(\mathbf{x}) & \text{if } |I_{outer}(\mathbf{x})| \leq \frac{1}{2} F d_{max} \\ M_{3\times3}(I_{outer}(\mathbf{x})) & \text{if } |I_{outer}(\mathbf{x})| > \frac{1}{2} F d_{max} \end{cases} \quad (7)$$

where $M_{3\times3}$ is a median filter of size 3×3.

Using the statistical properties of an image regarding the model (3), we describe the quality score qs_2 by means of ratios between means and standard deviations of y-lines in the derivation image $I_{dy}(x,y) \approx \frac{\partial I^{cleared}_{outer}(x,y)}{\partial y}$, defined as follows:

$$I_{dx}(x,y) = I^{cleared}_{outer}(x,y) - I^{cleared}_{outer}(x,y+1) \quad (8)$$

The quality score qs_2 is the sum of energies of ratios between means and standard deviations of y-lines in the derivation image $I_{dx}(x,y)$, as follows:

$$qs_2 = 100 - \min(100, 10(\sum_{y=1}^{h-1} |\frac{\text{mean}(I_{dx}(x,y), x \in (1,w))}{\text{std}(I_{dx}(x,y), x \in (1,w))}|^3)^{\frac{1}{3}}) \quad (9)$$

This metric makes use of the rather constant changes of the pixel values in the cleared fingerprint image, providing for low standard deviations compared to the mean in the y-lines in $I_{dx}(x,y)$, as long as the shaking occurred during the acquisition procedure. In case of high-quality scans, no-stripes are present in the $I_{dx}(x,y)$ and the changes are rather random, generating high standard deviations in comparison to the changes of the mean.

4. Results

In order to test the relevance of the proposed quality metrics, the following protocol was applied.

4.1. Ground truth for OCT quality estimation

400 samples of OCT scans of genuine fingerprints were randomly chosen from the database, and manually classified by an expert into two groups, $G_{acceptable}$ and G_{bad}, adhering to strict criteria as follows: (i) If some of the points on the outer fingerprint surface in the scan were closer than 30 voxels along the z-axis to the bottom of the volume, the scan was assigned to the group G_{bad}, as the scanner is unreliable in the part of the volume where $z \in (0, 30)$, and the situation results from the scenario when the finger was pressed too close to the surface of the sensor. (ii) If the surface of the outer fingerprint, as represented by the OCT scan, is suddenly discontinued after a specific value of the y-coordinate, the scan is assigned to the G_{bad} group (Fig. 6). Such a discontinuity pattern in the scan corresponds to lifting of the finger during the capture process. (iii) In order to describe the situation, where the strong shaking of the fingers occurred during scanning process, the scans are assigned to the G_{bad} group according to the following criteria; 1. The fingerprint surface is obviously disturbed by a function determined by a y-coordinate only. 2. The amplitude of the disturbances is clearly larger than than the amplitude of the ridge/valley pattern

All of the scans that do not satisfy any criteria required for the G_{bad} group, are considered to be of acceptable quality and assigned to the group $G_{acceptable}$.

4.2. Synthetically controlled OCT quality degradation

In order to perform synthetic degradation of the OCT scan quality, the pipeline of the layer estimation method is altered as follows. The outer fingerprint candidate-point set, S_{outer}, is extracted, representing the original high-resolution details of the surface of the outer fingerprint (Fig. 3b). A controlled quality degradation method is applied to the set, defined by the following equation ($Fd_{max} = 30$):

$$z = z + a(Fd_{max}SUR(\lfloor y/10 \rfloor) + 0.25Fd_{max}SUR(\lfloor y \rfloor)) \quad (10)$$

The function $SUR(x)$, generates random numbers from a uniform distribution, $SUR(x) \in (-0.5, 0.5)$, and cubically interpolates between $SUR(\lfloor x \rfloor)$ and $SUR(\lfloor x+1 \rfloor)$, if a non-integer value, $x \neq \lfloor x \rfloor$ is requested. The term $Fd_{max}SUR(\lfloor y/10 \rfloor)$ models the strong shaking pattern, while the term $Fd_{max}SUR(\lfloor y \rfloor)$ models the weak shaking pattern, whose variations are lower than the variations caused by the fingerprint pattern. The coefficient a represents amount of the degradation applied, where $a = 0$ represents no degradation and the original pattern is kept. After the degradation of S_{outer} is performed, the method normally proceeds with estimating the smooth surface f_{outer}.

4.3. OCT scan quality estimation

In order to assess relevance of the qs_1 quality score, one evaluation on synthetically degraded scans was carried out, along with one evaluation on the real low-quality scans. For the first scenario, the degradation model from the equation (10) was adopted.

If measured as the average distance between the estimated layer positions and the candidate point positions, $d_{outer} = \text{mean}(|z - f^{outer}(x,y)|) \wedge (x,y,z) \in S_{outer}$, the layer estimation method, run on the scans in $G_{acceptable}$, has achieved average d_{outer} of 3.06 with the standard deviation of 1.20.

The Fig. 9 illustrates the correlation, $c = -0.96$. between the level of the quality degradation, a, and the value of the quality score qs_1.

The real data evaluation was performed by assessing the ability of the quality score qs_1 to distinguish between the scans in the group $G_{acceptable}$ and the scans in the group G_{bad}, reported as false detection rates, as shown by Fig. 10.

A rigorous assessment of the relevance of the quality score qs_2 is challenging, as this score describes the fine variations caused by the slight shaking of the finger during the scanning, which variations are smaller than the variations caused by the presence of the fingerprint ridges and valleys. Nevertheless, the scans in the group $G_{acceptable}$ were fur-

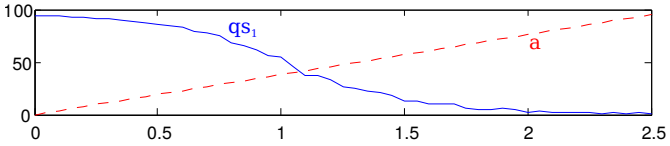

Figure 9. Quality score results on synthetically degraded data, a - quality degradation level, qs_1 - severe quality issues score

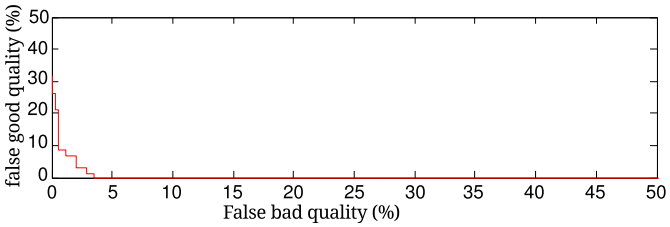

Figure 10. Detection results for the expert labeled ground truth data in terms of distinguishing between $G_{acceptable}$ and G_{bad}

ther manually classified, which classification was based on whether they contain a pattern caused by addition of a function depending solely on the y-coordinate. Such a pattern is observable by a closer examination of the scan, as the fingerprint pattern still appears disturbed by the weak shaking pattern in the y-coordinate only (Fig. 8). The classification results are illustrated by Fig. 11.

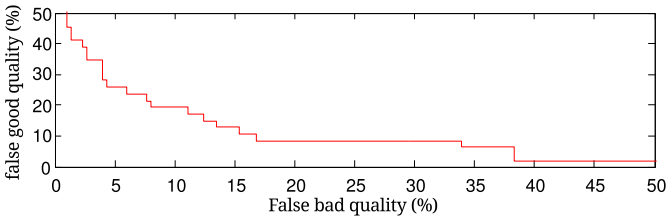

Figure 11. Results of detection of slight shaking of the scanned finger

5. Conclusions and future work

A reliable method for statistical approximation of the layer surfaces in an OCT fingerprint scan has been developed, allowing for extraction of the outer and inner fingerprint patterns. The method functions with a mean estimation error of 3.06 voxels and a standard deviation of the estimation of 1.2 voxels, which provides for a solid basis for extraction of the fingerprints into 2D representations. Two OCT-specific quality scores have been developed that enables discarding the low-quality scans that have resulted from a non-compliant capture subject behavior. For the more severe cases, the qs_1 allowed for detection of 98% of low-quality scans with a false detection rate of 3%.

The future work should focus on the application of the layer surface approximation method as a basis for the sweat gland identification and the subsequent verification of their genuine structure, providing for a reliable PAD method. The combination of the OCT-scan quality method proposed by this paper and a reliable PAD method would provide for a solid foundation for secure and reliable OCT-based fingerprint identification. A large-scale data collection performed by means of a high-quality OCT device of a larger scanning area is planned in the framework the project *OCT-Finger-II*. The full-area fingerprints that can be extracted from the resulting database will enable validation of the proposed quality scores in terms of the correlation with fingerprint recognition accuracy as defined in [6].

References

[1] S. Choi, T. Kim, and W. Yu. Performance evaluation of ransac family. In *Proc. BMVC*, pages 81.1–81.12, 2009.

[2] P. Coli, G. L. Marcialis, and F. Roli. Vitality Detection from Fingerprint Images: A Critical Survey. In *Proceedings of the international conference on Advances in Biometrics (ICB '07)*, page 722731, Berlin, Heidelberg, 2007.

[3] FANN. Fast artificial neural network library.

[4] L. Ghiani, P. Denti, and G. Marcialis. Experimental Results on Fingerprint Liveness Detection. In *Articulated Motion and Deformable Objects*, volume 7378 of *LNCS*, page 210218. 2012.

[5] L. Ghiani, D. Yambay, V. Mura, S. Tocco, G. Marcialis, F. Roli, and S. Schuckers. LivDet 2013 Fingerprint Liveness Detection Competition 2013. In *6th IAPR International Conference on Biometrics (ICB)*, 2013.

[6] ISO-IEC-29794-1. Biometric sample quality, 2009.

[7] D. Maltoni, D. Maio, A. K. Jain, and S. Prabhakar. *Handbook of Fingerprint Recognition*. Springer Publishing Company, Incorporated, 2nd edition, 2009.

[8] G. Marcialis, L. Ghiani, K. Vetter, D. Morgeneier, and F. Roli. Large Scale Experiments on Fingerprint Liveness Detection. In *Structural, Syntactic, and Statistical Pattern Recognition*, volume 7626 of *LNCS*, page 501509. 2012.

[9] D. W. Marquardt. An Algorithm for Least-Squares Estimation of Nonlinear Parameters. *SIAM Journal on Applied Mathematics*, 11(2):431–441, 1963.

[10] S. Meissner, R. Breithaupt, and E. Koch. Fingerprint fake detection by optical coherence tomography. In *SPIE 8571, Optical Coherence Tomography and Coherence Domain Optical Methods in Biomedicine XVII*, volume 8571, 2013.

[11] M. Menrath. Fingerprint with OCT. Master's thesis, Fern-Uniersität Hagen in Cooperation with Bundesamt für Sicherheit in der Informationstechnik (BSI), 2011.

[12] A. Munde. Biometrics and Security Evaluations. In *International Biometric Performance Conference (IBPC)*, 2012.

[13] OCT-Finger project. Bundesamt für Sicherheit in der Informationstechnik (BSI), Germany, 2010.

[14] C. Sousedik, R. Breithaupt, and C. Busch. Volumetric fingerprint data analysis using optical coherence tomography. In *International Conference of the Biometrics Special Interest Group (BIOSIG), 2013*, pages 1–6, Sept 2013.

[15] C. Sousedik and C. Busch. Presentation attack detection methods for fingerprint recognition systems: a survey. *Biometrics, IET*, x(x), 2014.